Journal of Power Sources 195 (2010) 4765–4771

Contents lists available at ScienceDirect

Journal of Power Sources

journal homepage: www.elsevier.com/locate/jpowsour

The influence of gas diffusion layer wettability on direct methanol fuel cell performance: A combined local current distribution and high resolution neutron radiography study

Alexander Schröder[a,*], Klaus Wippermann[a], Werner Lehnert[a], Detlef Stolten[a], Tilman Sanders[b], Thorsten Baumhöfer[b], Nikolay Kardjilov[c], André Hilger[c], John Banhart[c], Ingo Manke[c]

[a] Institute of Energy Research, IEF-3: Fuel Cells, Forschungszentrum Jülich GmbH, 52425 Jülich, Germany
[b] Institute for Power Electronics and Electrical Drives (ISEA), RWTH Aachen University, Jägerstr. 17–19, 52066 Aachen, Germany
[c] Helmholtz Centre Berlin (Hahn-Meitner-Institute), SF3, Glienicker Str. 100, 14109 Berlin, Germany

ARTICLE INFO

Article history:
Received 18 November 2009
Received in revised form 19 January 2010
Accepted 21 February 2010
Available online 26 February 2010

Keywords:
DMFC
High resolution neutron radiography
Current distribution
Fluid distribution
Wettability
GDL

ABSTRACT

The influence of the anode and cathode GDL wettability on the current and media distribution was studied using combined *in situ* high resolution neutron radiography and locally resolved current distribution measurements. MEAs were prepared by vertically splitting either the anode or cathode carbon cloth into a less hydrophobic part (untreated carbon cloth 'as received') and a more hydrophobic part (carbon cloth impregnated by PTFE dispersion). Both parts were placed side by side to obtain a complete electrode and hot-pressed with a Nafion membrane. MEAs with partitioned anode carbon cloth revealed no difference between the untreated and the hydrophobised part of the cell concerning the fluid and current distribution. The power generation of both parts was almost equal and the cell performance was similar to that of an undivided MEA (110 mW cm^{-2}, 300 mA cm^{-2}, 70 °C). In contrast, MEAs with partitioned cathode carbon cloth showed a better performance for the hydrophobised part, which contributed to about 60% of the overall power generation. This is explained by facilitated oxygen transport especially in the hydrophobised part of the cathode gas diffusion layer. At an average current density of 300 mA cm^{-2}, a pronounced flooding of the cathode flow field channels adjacent to the untreated part of GDL led to a further loss of performance in this part of the cell. The low power density of the untreated part caused a significant loss of cell performance, which amounted to less than 40 mW cm^{-2} (at 300 mA cm^{-2}).

1. Introduction

On the cathode side of a liquid fuelled DMFC, the flooding is more pronounced than in a PEFC, since the water is not only produced on the cathode side but permeates through the membrane additionally, driven by a concentration gradient and electroosmotic drag. On the anode side, the blocking effects of CO_2 bubbles may lead to a disturbance of the methanol supply. These two-phase flow effects do play a crucial role not only inside the GDL but also in the flow field channels. Due to the interaction between GDL and flow field, different GDLs result in altered fluid distributions inside the cell and therefore in different operating behaviours [1].

Uneven fluid distributions cause inhomogeneous current distributions which may lead to a significant power loss and accelerated degradation of the fuel cell. In order to investigate the effects leading to inhomogeneous current distributions, a measurement technique is mandatory, that allows the *in situ* observation of the current, CO_2 and water distribution simultaneously.

The use of segmented printed circuit boards (PCBs) is a well-established technique for measuring local currents in fuel cells. The features and advantages of our self-developed set-up, which is based on printed circuit board technology, are described in [2] (see also section 2). It allows the accurate measurement of up to 54 segment currents and impedances based on compensated sensor resistors [3].

Several methods have been reported in the literature to observe the CO_2 and water distribution *in situ* under operating conditions of PEFCs and DMFCs. Some authors used cells with a transparent cover to observe the carbon dioxide evolution and the two-phase flow behaviour visually. Transparent anode covers allow for the observation of different CO_2 flow patterns in DMFCs as a function of flow field design, current density, temperature, flow rate, pressure drop, and orientation [4–7]. A special set-up using a porphyrin dye compound reveals the distribution of oxygen in the cathode channels of a DMFC [8]. Observations of water transport phenomena in the cathode channels of PEFCs are also possible [9–11].

* Corresponding author. Tel.: +49 2461 61 1579; fax: +49 2461 61 6695.
E-mail address: a.schroeder@fz-juelich.de (A. Schröder).

0378-7753/$ – see front matter © 2010 Elsevier B.V. All rights reserved.
doi:10.1016/j.jpowsour.2010.02.057

A further method is synchrotron X-ray radiography [12–15]. This method allows the *in situ* observation of the fluid distribution in polymer membrane fuel cells on the micrometer scale with a resolution up to 3 μm. In the field of hydrogen fed PEFCs, the formation, growth and transport of water droplets have been studied [12–14]. Through-plane measurements of Manke et al. [12] proved the existence of different transport mechanisms: the first one via a continuous GDL pore filling, indicating a continuous "capillary-tree-like" transport, and the second one via an eruptive transport process. In-plane measurements of Hartnig et al. [13,14] enable a cross-sectional insight in the evolution and transport of water and thus a distinction between the different layers of the fuel cell. Both through-plane and in-plane techniques were applied to DMFCs under operating conditions [15]. The authors studied the carbon dioxide evolution and bubble formation at DMFC anodes. They found out that the dynamics of bubble formation and the detachment of bubbles from the position of formation strongly correlate with the current density [15].

In order to use a completely non-invasive method for the observation of CO_2 and water, we used neutron radiography which has proved its applicability for a variety of questions [16–22]. This method is based on the high attenuation coefficient of hydrogen compared to the attenuation coefficient of most metals and carbon. It means that the neutron beam can penetrate the metallic end plates and graphitic flow fields almost unattenuated, whereas liquid water leads to a strong attenuation of the beam. Thus, the distribution of hydrogen-rich species such as water and methanol can be observed during operation. Vice versa, areas where no liquid can be detected must be interpreted in terms of gas phase (air, carbon dioxide). In 1999, Bellows et al. used neutron radiography to study water transport profiles across Nafion in operating PEFCs [16]. Six years later, Kramer et al. investigated the two-phase flow inside the anodic compartment of an operating direct methanol fuel cell [17]. Manke et al. [18] presented a quasi-*in situ* neutron tomography on PEFC stacks including a cell-by-cell detection of liquid water agglomerates. A study of combined neutron radiography and locally resolved current density measurements of operating PEFCs was reported by Hartnig et al. [19]. They correlated the water distribution with the local activity of the respective area. In 2008, Manke et al. [20] investigated the liquid water exchange in two-phase flows within hydrophobic porous gas diffusion materials of PEFCs by spatially resolved hydrogen–deuterium contrast neutron radiography. Based on these results, they derived a new model for the water transport based on an eruptive mechanism. Hickner et al. [21] and Boillat et al. [22] carried out high resolution neutron radiography measurements using the in-plane imaging mode. They obtained detailed information on the cross-sectional water distribution in the MEA components and the gas flow channels. In our recent paper [23], the combination of *in situ* high resolution neutron radiography and segmented current distribution measurement was identified as a suitable tool to correlate current and fluid distribution in DMFCs. It was found that strongly inhomogeneous current distributions during cathodic flooding processes result in a performance loss of up to 30% of the initial value [23].

The intention of the present work is to study the influence of the anode and cathode GDL wettability on the current and media distribution using combined *in situ* high resolution neutron radiography and current distribution measurements. To visualize the difference between untreated and hydrophobised parts of the cell, either the anode or cathode GDL is vertically split into a less and a more hydrophobic part. The current distribution on the left and the right side of cells with undivided membrane electrode assemblies (MEAs) is approximately mirror-inverted, suggesting similar fluid distributions on the left and the right side of the cells. This is a condition precedent for the procedure of vertically splitting a GDL in two parts with a different hydrophobicity, because unequal current or media distributions on the left and the right part of the cell can be attributed to dissimilar hydrophobic properties of the two GDL parts. In contrast, a horizontal splitting of the GDLs would not be useful, since the media and current distribution of the upper and lower part of the cell is considerably different, caused by an accumulation of CO_2 in the top part of the cell and flooding in the middle and bottom part of the cell.

2. Experimental

2.1. Preparation of MEAs

The functional layers of the used MEAs with an active area of 4.2 cm × 4.2 cm were prepared onto carbon cloth (Ballard). The carbon cloth was used either as received or hydrophobised by impregnation with PTFE dispersion. Together with a microporous layer, the carbon cloths were used as gas diffusion layers for the electrodes. To compare hydrophobised and untreated GDLs in the same cell under operating conditions, either the anode or cathode GDL was vertically split into an untreated left part and a hydrophobised right part (see scheme in Fig. 1). To avoid an interaction of anode and cathode effects, the corresponding counter electrode was always undivided and hydrophobised.

As functional layers, first a hydrophobised microporous layer and then either the anode or cathode catalyst layer were prepared on the carbon cloth substrates by knife-over-roll technique. The microporous layer consisted of 60 wt.% carbon (Cabot, 2.1 mg cm^{-2}) and 40 wt.% PTFE (1.4 mg cm^{-2}). The anode catalyst consisted of 75 wt.% Pt/Ru and 25 wt.% carbon (Johnson Matthey). The Pt/Ru loading of the anodes was about 2 mg cm^{-2}. The cathode cata-

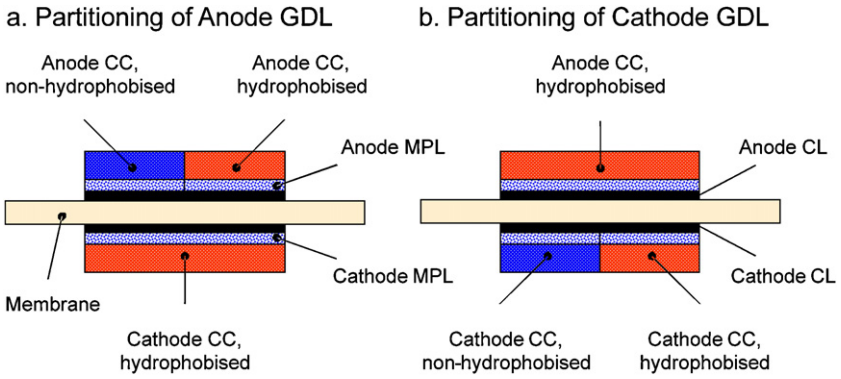

Fig. 1. Scheme of GDL partitioning by vertically splitting the carbon cloth into an untreated and a hydrophobised part. The neutron radiographs always represent the view from the cathode side. The splitting of anode and cathode was done in such a way, that the untreated carbon cloth always appears on the left hand side, and the hydrophobised carbon cloth is indicated in the right hand side of the neutron radiographs. *Abbreviations.* CC: carbon cloth; MPL: microporous layer; CL: catalyst layer.

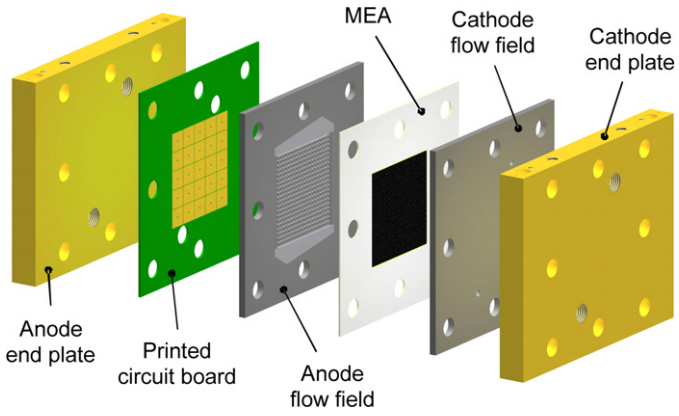

Fig. 2. Assembly of test cell. The printed circuit board is inserted between anode end plate and anode flow field.

lyst had a composition of 57 wt.% Pt and 43 wt.% carbon (Johnson Matthey) with a Pt loading of about 2 mg cm^{-2}.

The vertically splitting of the electrodes of the MEAs was realized by placing two GDE parts (each 2.1 cm × 4.2 cm), one with hydrophobised carbon cloth and the other one with untreated carbon cloth, side by side on a Nafion N-115 membrane to obtain a complete electrode (4.2 cm × 4.2 cm). On the other side of the membrane, the undivided counter electrode was placed. These three GDEs were subsequently hot-pressed on the membrane.

2.2. Electrochemical set-up and test cell

The experiments with partitioned GDLs were performed at different operating conditions and with a grid (column) flow field geometry. Each column has a cross-section of 1 mm × 1 mm and a height of 1 mm. Under counter flow conditions, air was fed at the top and methanol at the bottom of the cell. All measurements were carried out at a temperature of 70 °C and ambient pressure. The anode was constantly fed by a methanol solution with a concentration of 1 mol l^{-1} and a flow rate of 2.19 ml min^{-1}. The cathode was supplied with an air flow of 378 ml min^{-1}.

The current and temperature distribution was measured with a special measurement system, consisting of a printed circuit board (PCB) that was inserted between the aluminium end plate and the graphite flow field on the anode side (Fig. 2) and special electronics outside the cell. The PCB inside the cell assembly was equipped with a gold plated segmented contact area with 25 segments on the side towards the graphite flow field and one digital temperature sensor for each segment on the other side. The segmented contact area was connected with separate measurement and excitation wires to external electronics measuring the segment currents and controlling the potential of each segment so that all segments together form an equipotential surface in order to eliminate a smoothing of the current distribution caused by the measurement system, which would occur if only shunt resistors were used for measuring the segment currents. A detailed description of the measurement system can be found in [2].

This measurement system was also used to control the cell voltage and current by adjusting the voltage between the segmented contact area on the PCB and the cathode end plate. The whole measurement system was controlled with a central computer based sequential control program that also controlled the mass flow controllers for the air flow and the peristaltic pumps for the methanol flow.

A separate program was used to record the temperature reading from the temperature sensors on the PCB inside the cell and to display the temperature distribution.

2.3. Neutron radiography

The radiography experiments were performed at the neutron tomography instrument CONRAD/V7 at Helmholtz Centre Berlin (formerly Hahn-Meitner Institute) in Germany. The instrument is located at the end of a curved neutron guide which provides a cut-off for neutrons with wavelengths larger than 2 Å. In this way only the cold neutrons (spectral maximum at 3.5 Å) – which provide a much higher contrast than thermal neutrons – are transmitted through the neutron guide. High-energetic neutrons and gamma radiation are almost completely eliminated. The imaging set-up is based on a pinhole geometry where apertures with diameters from 1 cm to 3 cm can be used. For the performed experiments, an aperture with a diameter of 3 cm was used. The distance between the aperture and the sample is 5 m. The main part of the detector system is a 16-bit low-noise CCD camera (Andor DW436N with 2048 pixel × 2048 pixel) [24]. The camera is focused by a lens system on a neutron sensitive scintillator screen (Gadox – Gd_2O_2S:Tb) which was mounted close to the fuel cells (distance of 1 cm) to ensure high spatial resolutions down to 60 μm. The field of view was 60 mm × 60 mm in this case. The dynamic processes in the fuel cell were investigated by a time resolution of 15 s per image (10 s exposure time, 5 s readout).

For a better interpretation of the neutron radiographs, normalised radiographs are calculated: reference radiographs are taken with anode channels completely filled with methanol solution and cathode channels completely filled with air. The grey values of the radiographs taken during the measurements are divided by the grey values of the reference radiographs. That way, only the changes of a radiograph compared to the reference radiograph emerge. The formation of CO_2 in the anode channels results in a light grey value and the formation of liquid water in the cathode channels results in a dark grey value in the normalised radiograph.

3. Results

3.1. Influence of anode gas diffusion layer wettability

First of all, MEAs with vertically split anode carbon cloth were prepared and characterized. Fig. 3 shows normalised radiographs (left hand) and the corresponding current distributions (right hand) for three different average current densities and constant flow rates. All the neutron radiographs and current distributions shown in this figure were recorded under steady state conditions, i.e. after about 1 h. At the lowest average current density of 50 mA cm^{-2} and highest methanol and air stoichiometry of 24 (see Fig. 3a), only clusters of CO_2 bubbles appear in the anode flow field (see light spots). However, no flooding of cathode channels is observed under these conditions. The distribution of CO_2 bubbles across the anode is quite homogeneous: there is no visible difference between the left, untreated part (see blue frame) and the right, hydrophobised part (see red frame). The same is true for the current distribution, which appears to be more or less symmetrical. Thus, similar values of power generation are achieved for the left side (51%) and the right side (49%).

If the current density is increased to 150 mA cm^{-2} (see Fig. 3b), water droplets appear in the bottom part of the cathode channels (see dark spots), but there is virtually no difference between the untreated and the hydrophobised side. Again, similar currents and power densities are obtained for both parts of the MEA. The formation of water droplets in the bottom part of the channels may be explained by an increasing uptake of water vapour by the air stream from the top to the bottom of the cell. In case of a current density as low as 50 mA cm^{-2}, the small amount of water is solely removed

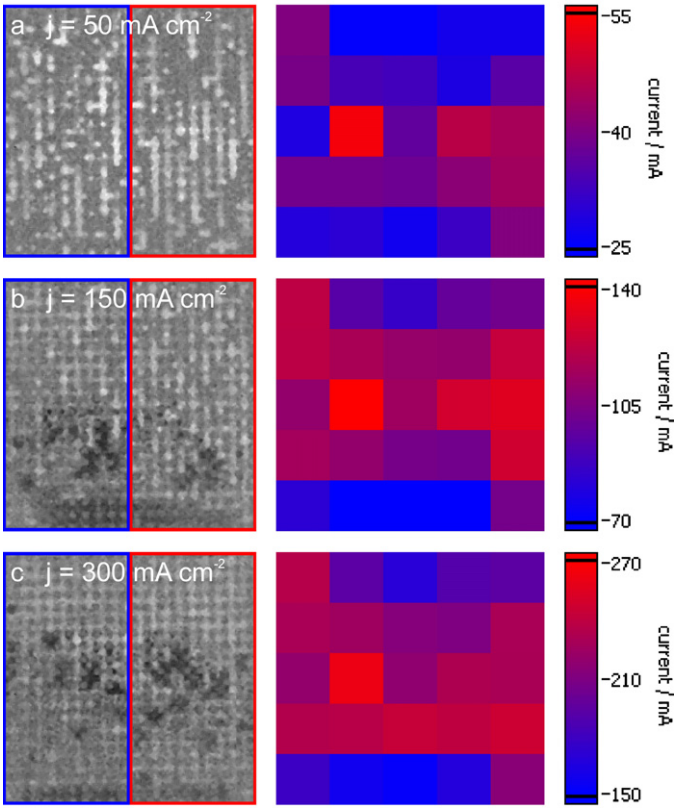

Fig. 3. Normalised radiographs (left hand) and the corresponding current distributions (right hand) of a MEA with a vertically split anode carbon cloth at current densities of 50 mA cm^{-2} (a), 150 mA cm^{-2} (b) and 300 mA cm^{-2} (c). Constant flow rates of 1 M methanol solution (2.19 ml min^{-1}) and air (378 ml min^{-1}), corresponding to methanol and oxygen stoichiometry factors of 24 (a), 8 (b) and 4 (c). All the neutron radiographs and current distributions were recorded under steady state conditions.

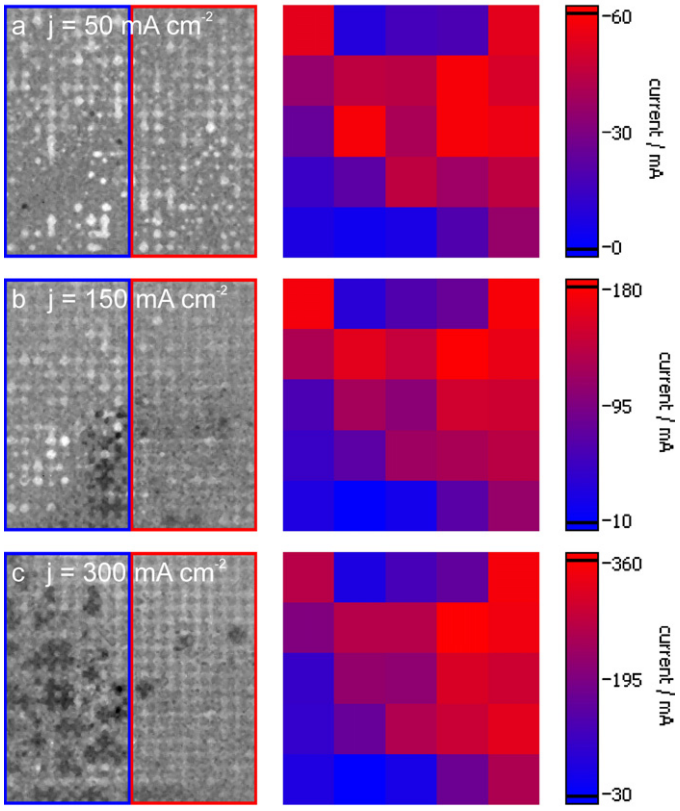

Fig. 4. Normalised radiographs (left hand) and the corresponding current distributions (right hand) of a MEA with a vertically split cathode carbon cloth, same operating conditions as described in the caption of Fig. 3.

as a gas: the dewpoint is not exceeded even in the bottom part of the cell, where the water concentration is highest (see Fig. 3a). If the current is increased from 50 mA cm^{-2} to 150 mA cm^{-2}, a threefold higher amount of water has to be removed by the same air volume. Under these experimental conditions, the dewpoint is exceeded at the so-called 'water boundary'. Above this boundary, water is removed as vapour. Below the upper boundary of the water droplets, oversaturation occurs and water droplets are generated in the cathode flow field channels (see Fig. 3b). The removal of water droplets is governed by gravitation (droplet size), capillary forces (GDL wettability properties and pore size distribution) and the interaction of water droplets with the wall of the cathode flow field channels (channel wettability properties and geometry).

At the highest current density of 300 mA cm^{-2} and the lowest air stoichiometry of 4, there is even more water in the cathode channels, preferentially in the middle part of the cell (see Fig. 3c). A tentative explanation for the latter observation is the increasing size of water droplets and their faster removal because of gravity, when they flow down and merge. Still, there is no significant difference concerning the liquid and current distribution between the untreated and hydrophobised part of the MEA. From the results of a vertically split anode GDL, it can be concluded that the wettability of anode carbon cloth only has a minor influence on the fluid transport in the DMFC anode. Therefore, MEAs with vertically split anode carbon cloth have the same performance (110 mW cm^{-2}, 300 mA cm^{-2}) as undivided MEAs with hydrophobised anode carbon cloth.

3.2. Influence of cathode gas diffusion layer wettability

The same experiments were performed by vertically splitting the cathode carbon cloth. Again, the neutron radiographs and the corresponding current distributions are shown for three different average current densities (see Fig. 4). As above, only the data obtained under steady state conditions are shown. At the lowest current density of 50 mA cm^{-2}, only the evolution of CO_2 bubbles, but not the formation of water droplets in the cathode gas channels is observable (see neutron radiograph in Fig. 4a). Nevertheless, there is a dominant power generation of about 60% in the right, hydrophobised part of the cell (see current distribution in Fig. 4a). Hence, there is no correlation between the fluid distribution shown in the neutron radiograph and the current distribution under these conditions. This result indicates that it is not only the fluid distribution in the flow field channels that has to be considered, but also the media distribution in the underlying porous gas diffusion electrodes, which cannot be resolved in these experiments and which is also supposed to have a large influence on current distribution. Most probably, a partial flooding of the untreated carbon cloth in the left side of the MEA and subsequent blocking of the oxygen transport is responsible for the low performance of this part.

If the average current density is increased to 150 mA cm^{-2}, water droplets appear preferentially in the left, untreated part of the cathode channels. Again, the left part of the cell contributes to 40% of the overall power generation only. The time-dependent current density, power density and cell voltage during the experiment are presented in Fig. 5. Concerning current and power density, the total values as well as the data of untreated (left) part and hydrophobised (right) part are shown. As the total current is constant during the experiment, inverse curves of the currents in the untreated and the hydrophobised part of the cell are indicated in

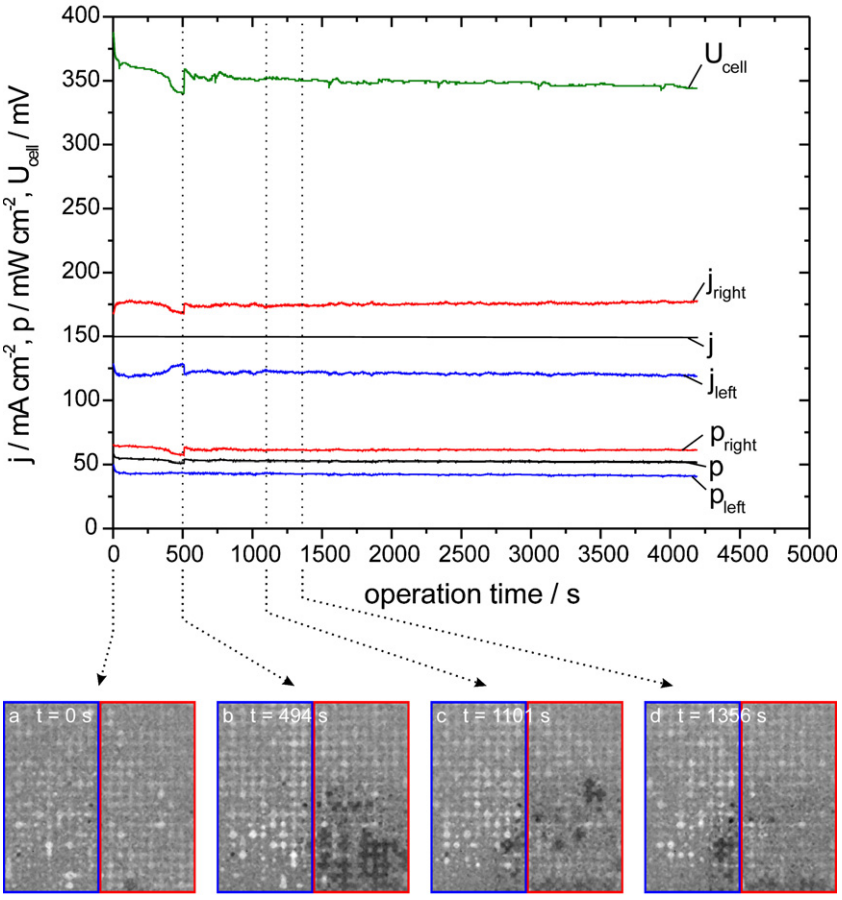

Fig. 5. Time dependence of current density, power density and cell voltage during the experiment performed at a current density of 150 mA cm^{-2} with the MEA containing a vertically split cathode carbon cloth (see Fig. 4b). In case of current and power density, total values as well as data of untreated (left) part and hydrophobised (right) part are presented. Additionally, neutron radiographs indicating characteristic states of media distribution in the flow field channels are shown.

Fig. 5. Additionally, neutron radiographs are shown for different, time-dependent states of media distribution in the flow field channels. They can be compared with a neutron radiograph taken at steady state conditions in Fig. 4b.

Immediately after switching on the current, only very few, small water droplets are visible in the neutron radiograph (see Fig. 5a, $t = 0$ s). In the following period up to about 500 s, the cell voltage, power density and current of the hydrophobised part drops, whereas the current of the untreated part increases. This is due to a flooding of the right, hydrophobised part of the cell during that time and demonstrated by the neutron radiograph taken after 494 s, showing water droplets generated in the bottom, right part of the cathode flow field channels. After 500 s of operation, most of the water droplets disappear (not shown here). Simultaneously, U_{cell}, p, p_{right} and j_{right} increase and j_{left} decreases. The enhanced performance can easily be explained by an improved oxygen supply of the right, hydrophobised part of the cell. However, it should be emphasised that the current in the hydrophobised part of the cell is always higher than that in the untreated part, independent on visible flooding effects in the flow field channels. This result again suggests that water management of GDLs can be even more important than the liquid distribution in the flow field channels. It further suggests future experiments to be performed not only in the through-plane mode, but also in the cross-sectional viewing direction to visualize the liquid distribution within the GDLs. This means neutron radiography as well as synchrotron X-ray investigations.

As the experiment goes on, more and more water droplets appear in the left, untreated part of the cell (see neutron radiograph Fig. 5c). After about 1300 s, steady state conditions are achieved with some agglomeration of water droplets in the left part of the cell and almost constant cell performance. Thus, the neutron radiographs in Fig. 5d (1356 s) and Fig. 4b (end of experiment) are quite similar.

The effects of water accumulation in the left part of the cathode flow field channels and the lower power generation in this part of the cell are even more pronounced at the highest average current density of 300 mA cm^{-2}, shown in Fig. 4c. Water droplets appear in the cathode channels over the entire left side of the cell, causing an additional power loss: the untreated part of the cell contributes to 38% of the total power generation only. Fig. 6 shows the time-dependent performance data for the average current density of 300 mA cm^{-2}. Qualitatively, the same behaviour is obtained as compared to the results achieved at an average current density of 150 mA cm^{-2} (see Fig. 5). However, the flooding of the right, hydrophobised part of the cathode flow field (see neutron radiograph Fig. 6b) and the sudden removal of the water droplets are three times faster and the change of performance during these processes is more pronounced. After about 270 s (see neutron radiograph Fig. 6c), the amount of water in the cathode flow field channels of the left and the right part of the cell are approximately the same. It takes about 460 s, until steady state conditions are achieved and the water droplets predominantly appear in the left, untreated part of the cell (see neutron radiograph Fig. 6d).

No conclusive explanation for the observed 'shift' of water droplets in the cathode channels from the hydrophobised to the untreated part of the cell can be offered here. However, the three times faster process when doubling the current density suggests a mechanism, where the untreated part of the GDL behaves like a

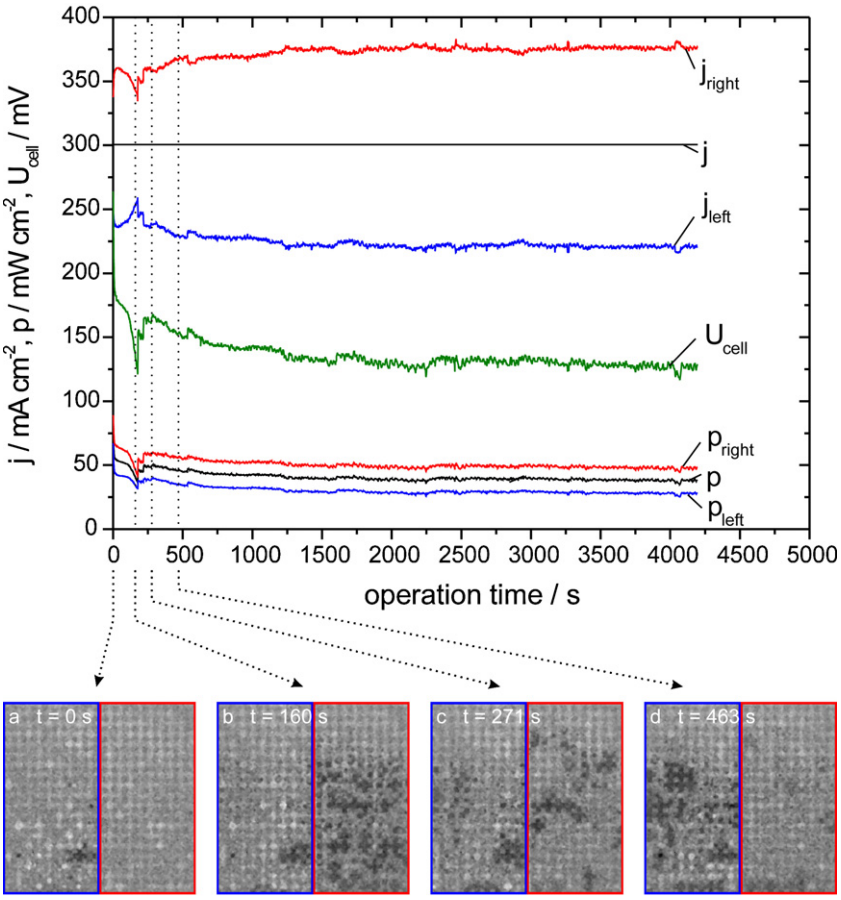

Fig. 6. Time dependence of current density, power density and cell voltage during the experiment performed at a current density of 300 mA cm^{-2} (compare Fig. 4c), same MEA and operating conditions as described in Fig. 5.

sponge, taking up water in the beginning of the experiment after switching on the current. Therefore, water removal preferentially takes place in the cathode flow field channels of the hydrophobised part of the cell during this period. When the water uptake capacity of the untreated GDL is exceeded, water droplets are released to the cathode flow field channels in this part of the cell. The higher the current density, the more water is produced in the cathode gas diffusion electrode and the faster is the process of taking up water in the untreated part of the cathode GDL.

The MEA with divided cathode carbon cloth has a performance of less than 40 mW cm^{-2} (300 mA cm^{-2}) under steady state conditions, which is only little more than one-third of the performance of undivided, standard MEAs under these conditions. This result can be explained by the restricted oxygen transport in the left, untreated part of the cell due to water accumulation in the cathode GDL and flow field channels, causing a high cathode overpotential and a cell voltage drop. It means that the actual, low performance of the untreated part dominates the total power density of the cell.

4. Conclusions

The combination of high resolution neutron radiography and simultaneous measurement of the local current distribution provides valuable information about the influence of GDL wettability on the performance of a DMFC. It turns out that the hydrophobicity of the anode carbon cloth has practically no influence on the fluid transport in the DMFC anode and thus the performance of the MEA. In contrast, hydrophobisation of the cathode carbon cloth seems to be important, as it enables a fast removal of water droplets, facilitates the oxygen transport in the cathode GDL and cathode flow field channels and thus increases the performance. This effect is even more pronounced at high current densities. Under the above-mentioned operating conditions, the fluid distribution in the porous layers of the gas diffusion electrodes appears to be crucial for the local cell performance. The water distribution in cathode GDLs cannot be resolved by neutron radiography when operating in through-plane mode. In order to visualize local flooding processes in cathode GDLs, it is suggested to perform future experiments with neutron radiography and/or synchrotron X-ray investigations in the cross-sectional viewing direction.

Acknowledgement

We gratefully acknowledge the financial support of this work by the German Federal Ministry of Education and Research (BMBF) under Grant No. 03SF0324.

References

[1] C. Hartnig, L. Jörissen, W. Lehnert, J. Scholta, in: M. Gasik (Ed.), Direct Methanol Fuel Cells (DMFC), Materials for Fuel Cells, Woodhead Publishing Limited, 2008, pp. 185–208.
[2] D.U. Sauer, T. Sanders, B. Fricke, T. Baumhöfer, K. Wippermann, A.A. Kulikovsky, H. Schmitz, J. Mergel, Journal of Power Sources 176 (2008) 477–483.
[3] T. Sanders, T. Baumhöfer, D.U. Sauer, A. Schröder, K. Wippermann, ECS Transactions 25 (2009) 1719–1728.
[4] P. Argyropoulos, K. Scott, W.M. Taama, Electrochimica Acta 44 (1999) 3575–3584.
[5] H. Yang, T.S. Zhao, Q. Ye, Journal of Power Sources 139 (2005) 79–90.
[6] C.W. Wong, T.S. Zhao, Q. Ye, J.G. Liu, Journal of the Electrochemical Society 152 (2005) A1600–A1605.
[7] Q. Liao, X. Zhu, X. Zheng, Y. Ding, Journal of Power Sources 171 (2007) 644–651.

[8] J. Inukai, K. Miyatake, Y. Ishigami, M. Watanabe, T. Hyakutake, H. Nishide, Y. Nagumo, M. Watanabe, A. Tanaka, Chemical Communications (2008) 1750–1752.
[9] X. Liu, H. Guo, C. Ma, Journal of Power Sources 156 (2006) 267–280.
[10] X. Liu, H. Guo, F. Ye, C. Ma, Electrochimica Acta 52 (2007) 3607–3614.
[11] D. Spernjak, S.G. Advani, A.K. Prasad, Journal of the Electrochemical Society 156 (2009) B109–B117.
[12] I. Manke, C. Hartnig, M. Grünerbel, W. Lehnert, N. Kardjilov, A. Haibel, A. Hilger, J. Banhart, H. Riesemeier, Applied Physics Letters 90 (2007) 174105.
[13] C. Hartnig, I. Manke, R. Kuhn, N. Kardjilov, J. Banhart, W. Lehnert, Applied Physics Letters 92 (2008) 134106.
[14] C. Hartnig, I. Manke, R. Kuhn, S. Kleinau, J. Goebbels, J. Banhart, Journal of Power Sources 188 (2009) 468–474.
[15] C. Hartnig, I. Manke, J. Schloesser, P. Krüger, R. Kuhn, H. Riesemeier, K. Wippermann, J. Banhart, Electrochemistry Communications 11 (2009) 1559–1562.
[16] R.J. Bellows, M.Y. Lin, M. Arif, A.K. Thompson, D. Jacobson, Journal of the Electrochemical Society 146 (1999) 1099–1103.
[17] D. Kramer, E. Lehmann, G. Frei, P. Vontobel, A. Wokaun, G.G. Scherer, Nuclear Instruments and Methods in Physics Research A 542 (2005) 52–60.
[18] I. Manke, C. Hartnig, M. Grünerbel, J. Kaczerowski, W. Lehnert, N. Kardjilov, A. Hilger, J. Banhart, W. Treimer, M. Strobl, Applied Physics Letters 90 (2007) 184101.
[19] C. Hartnig, I. Manke, N. Kardjilov, A. Hilger, M. Grünerbel, J. Kaczerowski, J. Banhart, W. Lehnert, Journal of Power Sources 176 (2008) 452–459.
[20] I. Manke, C. Hartnig, N. Kardjilov, M. Messerschmidt, A. Hilger, M. Strobl, W. Lehnert, J. Banhart, Applied Physics Letters 92 (2008) 244101.
[21] M.A. Hickner, N.P. Siegel, K.S. Chen, D.S. Hussey, D.L. Jacobson, M. Arif, Journal of the Electrochemical Society 155 (2008) B427–B434.
[22] P. Boillat, D. Kramer, B.C. Seyfang, G. Frei, E. Lehmann, G.G. Scherer, A. Wokaun, Y. Ichikawa, Y. Tasaki, K. Shinohara, Electrochemistry Communications 10 (2008) 546–550.
[23] A. Schröder, K. Wippermann, J. Mergel, W. Lehnert, D. Stolten, T. Sanders, T. Baumhöfer, D.U. Sauer, I. Manke, N. Kardjilov, A. Hilger, J. Schloesser, J. Banhart, C. Hartnig, Electrochemistry Communications 11 (2009) 1606–1609.
[24] N. Kardjilov, A. Hilger, I. Manke, M. Strobl, W. Treimer, J. Banhart, Nuclear Instruments and Methods in Physics Research A 542 (2005) 16–21.